



THE UNIVERSITY *of* EDINBURGH

## Edinburgh Research Explorer

### Diffusion of volatiles in hot stagnant-lid regime planets

**Citation for published version:**

Bromiley, G 2019, 'Diffusion of volatiles in hot stagnant-lid regime planets', *Planetary and space science*.  
<https://doi.org/10.1016/j.pss.2019.104822>

**Digital Object Identifier (DOI):**

[10.1016/j.pss.2019.104822](https://doi.org/10.1016/j.pss.2019.104822)

**Link:**

[Link to publication record in Edinburgh Research Explorer](#)

**Document Version:**

Peer reviewed version

**Published In:**

Planetary and space science

**General rights**

Copyright for the publications made accessible via the Edinburgh Research Explorer is retained by the author(s) and / or other copyright owners and it is a condition of accessing these publications that users recognise and abide by the legal requirements associated with these rights.

**Take down policy**

The University of Edinburgh has made every reasonable effort to ensure that Edinburgh Research Explorer content complies with UK legislation. If you believe that the public display of this file breaches copyright please contact [openaccess@ed.ac.uk](mailto:openaccess@ed.ac.uk) providing details, and we will remove access to the work immediately and investigate your claim.



# **Diffusion of volatiles in hot stagnant-lid regime planets**

**Geoffrey D. Bromiley**

**School of GeoSciences, University of Edinburgh, King's Buildings, Edinburgh EH9**

**3FE, UK**

**geoffrey.bromiley@ed.ac.uk**

**+44 (0)131 650 8519**

**Key words: stagnant lid; Venus; water; diffusion; exoplanet; volatile**

## **Abstract**

Earth is unique within our solar system in having a convective regime dominated by plate tectonic processes. More typical of rocky, 'terrestrial' planets is a "stagnant lid" regime, where the entire lithosphere is a single plate, variably punctured by plume-driven volcanic activity. As such, a significant fraction of 'Earth-like' exoplanets might instead have stagnant lids. For hot stagnant lid planets like Venus, high temperatures towards the base of the lid mean that solid-state diffusion potentially provides a mechanism for redistributing lighter, faster-diffusing volatile elements such as H. To investigate the importance of this mechanism a 1-d model is used to constrain volatile flux from a relatively undegassed planetary interior into a hot stagnant lid. Diffusion only results in significant flux of H through an oxidised lid; diffusion of H in reduced stagnant lids and diffusion of other volatile elements, is inconsequential. For modelled Venusian temperature profiles H diffusion fronts progress a limited distance (10s of km) into the lid over Gyr timescales. However, for a small relative increase in lid temperature (i.e. a slightly hotter than Venus exoplanet), H diffusion into the lid becomes considerable over shorter timescales. H flux upwards into the lid eventually stagnates with decreasing

temperature. However, H flux markedly reduces mantle solidus in lower portions of the lid, decreasing lid stability and promoting lid rejuvenation. Given the influence of H on a range of mantle properties from melt relations to rheology, future models of stagnant lid planetary evolution should assess the role of diffusion in redistributing H.

## **1. Introduction**

Over the past decade, a marked increase in detection rate of extrasolar planets has led to the identification of numerous “Earth-like” exoplanets (e.g. Coughlin et al., 2016; Dragomir et al., 2019; Gillon et al., 2012), i.e. planets with similar mass and radius to the Earth. This has driven research into issues related to planetary habitability, controls on the initiation of plate tectonics, interplay between geological processes and atmospheric evolution, and the wider issue of what ‘Earth-like’ actually means (Angelo et al., 2017; Barstow et al., 2016; Dittmann et al., 2017; Dorn et al., 2018; Foley, 2018; Foley and Driscoll, 2016; Rushby et al., 2018; Shahr et al., 2019; van Summeren et al., 2011). Within our own solar system Earth is one of 4 ‘rocky’ planets which have iron-rich cores surrounded by shells of silicate. However, among these it is unique in having a geological evolution dominated by plate tectonic processes (O’Rourke and Korenaga, 2012). The lithosphere of Earth is divided into a number of discrete plates. Relative movement of these plates stimulates planet-wide geochemical recycling via subduction, gives rise to magmatism in addition to plume-related mantle melting, and may buffer Earth’s hydrosphere and atmosphere by controlling flux of volatile elements such as H<sub>2</sub>O and CO<sub>2</sub>. In contrast, Mercury, Venus, Mars and other bodies such as the Moon and Io are ‘single plate’ (Johnson and Hauck II, 2016; Plesa et al., 2018; Smrekar et al., 2018; Veeder et al., 2009; Wieczorek et al., 2006) and have convective regimes in which a thick ‘stagnant lid’ overlies the convecting mantle, at least until the point where heat loss renders bodies geologically inactive. Plume-related upwellings within a stagnant lid regime dominate volcanic activity and interior-to-surface flux of material, and limited recycling of material back into the deep interior is only possible by delamination of the

parts of the lid or localised lid melting (Elkins-Tanton et al., 2007), although limited subduction has been proposed on Venus (Schubert and Sandwell, 1995) possibly related to plume upwelling (Davaille et al., 2017). Conditions which result in the development of a global plate tectonic regime remain uncertain, although the fact that they occurred on Earth alone indicates that many ‘Earth-like’ exoplanets could be ‘Venus-like’, and although similar to Earth in terms of size and mass, may have stagnant lid convective regimes (Kane et al., 2018; Smrekar et al., 2018).

Although similar in terms of size and density to the Earth, there is no evidence for global plate tectonic processes on Venus. Instead, a single plate of thick buoyant lithosphere is assumed to inhibit mantle upwelling and active magmatism (Nimmo and McKenzie, 1998; Smrekar et al., 2018). There is ongoing debate as to whether Venus is in a stable stagnant lid regime or a regime punctuated by brief episodes of lid overturn and global resurfacing, although numerical models suggest that even if Venus is within an episodic regime it is likely to have had a stable stagnant lid for >500 Myr (Rolf et al. 2018). A stable stagnant lid is punctured only by volcanic processes related to upwelling plumes (Solomatov and Moresi, 1996), resulting in a surface dominated by basaltic magmatism related to plume-driven mantle melting (Ivanov and Head, 2015). In end-member stagnant lid regime planets volcanism provides the main mechanism for transporting volatiles such as H<sub>2</sub>O and CO<sub>2</sub> out of the deep interior, i.e. mantle ‘degassing’. In the absence of large-scale subduction of lithosphere, flow of volatiles can be considered largely uni-directional.

The upper atmosphere of Venus is extremely dry (Bertaux et al., 2007). Even accounting for H loss due to photodissociation (Lecuyer et al., 2000), atmospheric water contents are orders of magnitude lower than the amount of surface water on Earth. This observation, and the apparent stiffness of the Venusian crust, have been used to argue that the interior of Venus is largely anhydrous (Elkins-Tanton et al., 2007; Nimmo and McKenzie, 1998). In

contrast to the Earth, Venus could have either lost volatiles such as H<sub>2</sub>O over the past 4 Gyr by volcanic degassing, or accreted volatile-free. However, Venus Express data indicates that the lower atmosphere of Venus could be variably water-rich (Bezard et al., 2009). Mantle degassing on Venus is also estimated to be an inefficient process at best (e.g. Kaula, 1999; Lecuyer et al., 2000; Mikhail and Heap, 2017). Furthermore, models of planetary accretion demonstrate that Venus and Earth should have similar volatile budgets (Wetherill GW, 1986). This is supported by gamma-ray spectroscopic data on lithophile element ratios, which indicate that Venus, Mars and Mercury accreted comparable or greater H than Earth, relative to marked depletions for the Moon and 4 Vesta (Greenwood et al., 2018). Given (1) that that most terrestrial volatiles were delivered during initial accretion of the Earth (Altwegg et al., 2015; Marty et al., 2017) and (2) that even the Moon-forming impact did not drive volatile-loss in the early Earth-Moon system (Saal et al., 2008, 2013), it follows that other inner solar system planets also accreted appreciable volatiles. As such, it appears likely that the interior of Venus was originally volatile-bearing, has remained relatively hydrous and volatile-rich. An H<sub>2</sub>O and CO<sub>2</sub>-bearing Venusian interior is also supported indirectly by evidence for pyroclastic volcanism (Airey et al. 2015; Campbell et al., 2017), and by geochemical modelling of limited surface composition data from Venera and Vega landers (Filiberto, 2014).

Regardless of arguments for or against a volatile-bearing Venusian interior, it is probable that a significant fraction of Earth-size/mass stagnant-lid regime exoplanets have volatile-bearing interiors. Recent studies have investigated flux of H<sub>2</sub>O and CO<sub>2</sub> in Earth-like stagnant lid exoplanets, largely in terms of implications for planetary habitability (e.g. Foley and Smye, 2018; Noack et al., 2017; Tosi et al., 2017). As well as being of key importance in understanding why Earth or other planets might support life, H<sub>2</sub>O (or H) also has a disproportionate influence on a range of terrestrial mantle properties, from rheology to melting behaviour (Peslier, 2010, and references therein). As such, H has a pivotal role in

understanding planetary processes more widely. The extent to which volatiles such as H<sub>2</sub>O might both influence, and be influenced by processes occurring within stagnant-lid regime planets remains largely unknown, although variable water contents have been used to explain viscosity variations in numerical models (e.g. Rolf et al., 2018). Volatile element redistribution on Venus is typically considered solely in terms of volcanic degassing (e.g. O'Rourke and Korenaga, 2012; Smrekar and Sotin, 2012; Wordsworth, 2016). However, for hot stagnant planets, (1) the inferred stability of stagnant lids over long periods of time (Gyr), (2) high temperatures across the lower portions of the lid (e.g. Ghail, 2015), (3) the possibility that volatile distribution across planetary interiors is heterogenous after planet formation, and (4) fast diffusivities of species such as H, raise the possibility that solid state diffusion provides an additional mechanism for redistributing light, volatile species in undegassed planetary interiors. Solid state diffusion is an inherently slow process and will not influence element redistribution within freely convecting regions of planetary interiors. However, diffusion is highly temperature dependent, and over geological timescales can contribute to redistribution of lighter, more mobile elements, for example, into or out of lower portions of a hot stagnant lid. Although this would likely represent an insignificant mechanism in terms of total volatile element loss from an undegassed planetary interior, progressive flux of elements such as H could have an important influence on lid stability through time. Biased discovery of exoplanets orbiting close to parent stars, and on the inner margin of within stellar habitable zones (Kane et al., 2018) means that consideration of the relative importance of diffusion in Venusian or 'hot Venusian' exoplanets is timely.

## **2. Method**

A stagnant lid can be envisioned as a complex polycrystalline, multi-phase material. In a material such as this diffusivity of volatiles such as H will vary significantly as a function of temperature, mineralogy, mineral chemistry, oxygen fugacity, grain size and grain boundary width. However, these factors in turn, especially temperature, vary vertically upwards across

the stagnant lid. As such, diffusivity across the lid will vary by orders of magnitude in a non-uniform manner. Thermal evolution of the lid will likewise result in progressive changes in diffusivity across the lid.

In order to provide first constraints on the extent to which diffusion redistributes volatiles across a hot, geologically complex stagnant lid, I develop here a 1D model. The model assumes that the initial distribution of volatiles across the interior of a broadly Venus-like interior is heterogeneous, and that a stagnant lid depleted in volatile elements overlies a relatively undegassed convecting mantle. As such, the model imparts a concentration gradient sufficient to drive flux of volatiles into the lid. A box model is then developed to constrain, using data from experimental studies, how diffusivity varies with depth through the lid as a function of temperature. This model is time-independent, and assumes that the lid and temperature profile remain unchanged. In an evolving planet, the temperature profile across the lid, and lid thickness itself, will vary with time (e.g. Rolf et al., 2018). However, given that solid state diffusion is an inherently slow process only expected to be significant over long timescales (>100 Myr), smaller temperature fluctuations are buffered within the model, and temperature profiles across the lid can be considered as an average set of conditions over time in a mature stagnant-lid regime planet.

## **2.1 Conceptual stagnant lid model**

For the model, a simplified stable stagnant lid structure based on that of O'Rourke and Korenaga (2015) was used, based on the internal structure of a Venus. In this model (figure 1), a 170km thick stagnant lid consists of 30 km of basaltic crust overlying a mantle lithospheric component. This 2-component lid overlies a convecting mantle. Thickness of the lid, division into crustal and mantle lithospheric components, and a upper surface temperature of 735 K are all based on inferred models for present day Venus (e.g. Nimmo and McKenzie, 1998), although the model is broadly representative of a rocky (i.e. terrestrial)

body with a thick, stable stagnant lid. The model used here assumes that the convecting mantle is relatively undegassed, and as such, due to its volume can be considered an infinite reservoir for volatiles. The stagnant lid is assumed to be initially volatile-free (or volatile poor for later models). This is based on the assumption that incompatible volatile elements would partition into primary mantle melts, thereby forming basaltic crust and variably degassing to the atmosphere, with the remainder of the lid comprised of melt residue, and essentially stripped of volatile species. Although an obvious simplification, this model provides a useful system for exploring volatile flux into a hot stagnant lid. The broad concept of a volatile-free lid overlying a progressively more volatile enriched deep interior is, furthermore, in line with experimental studies which demonstrate that 'water', i.e. H<sub>2</sub>O, storage capacity is proportional to water fugacity to the power  $n$ ,  $f_{\text{H}_2\text{O}}^n$ , and as such, increases markedly with depth (Bolfan-Casanova, 2005; Bromiley et al., 2004; Bromiley and Keppler, 2004; Rauch and Keppler, 2002). The model used here can be modified to explore the effect of different initial volatile element distributions, and different stagnant lid compositions and proportions. In the model, the lid mantle component is a 2-mineral mix 60% olivine + 40% orthopyroxene with a 3 mm grain size; this simplified hazburgite composition represents a mantle residue from which 15-25% basaltic liquid has been extracted. However, it is also broadly representative of any ultramafic, peridotitic (olivine-rich) composition. The overlying basaltic crust, which is not expected to contribute to volatile flux but is added here for the sake of completion, is modelled as a 2-mineral mix of 60% pyroxene + 40% plagioclase with a 1 mm grain size. Grain sizes are estimated based on personal observations of gabbroic and hazburgitic units in ophiolitic sequences, and in line with inferred grain sizes in published studies (Demouchy et al. 2010a,b; Bromiley and Hiscock, 2016). Minerals are assumed to be randomly oriented in both lid components, Variation in temperature with depth through the stagnant lid is modelled based on published models of the interior structure of Venus, as discussed below. Variation in temperature, and to a much lesser extent pressure, coupled to changes in mineralogy within the lid results in significant variations in diffusivity of each species with



depth. To constrain this variation, the model lid is divided into a series of 10 km thick shells. Bulk temperature within each shell is constrained by the temperature profile, and a representative diffusivity for each species in each phase calculated. For each shell, a weighted bulk diffusivity can then be determined. In this manner, non-trivial variations in diffusivity across a simultaneous concentration gradient can be simulated, which is the key feature of any realistic model for volatile flux into a stagnant lid. A limitation in this approach is that temporal variations such as evolution in the temperature gradient across the stagnant lid or the proportions of the stagnant lid itself, cannot be simulated, although multiple temperature profiles can be used to assess the effects on changes in lid temperature with time. Furthermore, slow diffusion of volatiles over 100 Myr+ durations means that shorter duration temperature variations are buffered over long timescales; as such, temperature profiles used here can be considered as average conditions over the timescales used within the model.

## **2.2 Modelling hydrogen diffusivity**

Due to its small mass and incorporation mechanisms in silicates, H is the fastest diffusing volatile species under relevant deep planetary conditions. As such, H will be the volatile most likely to be mobilised within a solid, stagnant lid regime planet. Hydrogen is typically incorporated in nominally anhydrous mantle minerals as interstitial  $H^+$ , charge balanced by metal vacancies or substitutional defects (Bell and Rossman, 1992; Bolfan-Casanova, 2005; Ingrin and Skogby, 2000). Diffusion of  $H^+$  requires coupled diffusion of some other species to maintain charge neutrality, and the nature of this species will influence  $H^+$  diffusivity.  $H^+$  diffusion in olivine was modelled here using data from Mackwell and Kohlstedt (1990) who constrained diffusivity of  $H^+$  coupled to counter flux of polarons (i.e. reduction of  $Fe^{3+}$  to  $Fe^{2+}$ ). H flux modelled using this data assumes availability of  $Fe^{3+}$ , or in other words, a relatively oxidised stagnant lid. Limited data on the geochemistry of the Venusian lid suggests that this is a reasonable assumption. Wordsworth (2016) proposed that photolysis of  $H_2O$  in the early

Venusian atmosphere liberated O and H. During subsequent H loss to space, the Venusian mantle would have been progressively oxidised by atmospheric interaction with the remaining O. Wordsworth (2016) calculated that this redox pump mechanism will have oxidised the Venusian mantle to approximately the magnetite-hematite buffer. Similarly, Lecuyer et al. (2000) argued that the simultaneously high D/H and low H<sub>2</sub>O content for the Venusian atmosphere compared to Earth is consistent with either significant hydration of the Venusian crust, or photolysis of H<sub>2</sub>O, H loss and mantle oxidation. Regardless of this, it is likely that all large (i.e. Earth/Venus sized) rocky planets undergo some degree of self-oxidation during the latter stages of planetary formation. Bodies larger than Mars have a sufficient size to form a substantial silicate perovskite-dominated lower mantle. The perovskite-structured mineral bridgmanite, (Mg,Fe)<sub>2</sub>SiO<sub>3</sub>, will be the dominant lower mantle mineral over a wide range of compositions, and importantly, has been shown to freely dissociate Fe<sup>2+</sup> into Fe metal and Fe<sup>3+</sup> (Frost et al., 2004). Crystallisation of bridgmanite during magma ocean solidification should, therefore, act as a mechanism for self-oxidation in large rocky planets soon after their formation, regardless of later/additional mechanisms for mantle oxidation. A similar mechanism for self-oxidation and iron disproportionation has also been noted in high pressure experiments on garnet and pyroxene-bearing lithologies (Rohrbach et al., 2007). As such, the condition that there is sufficient Fe<sup>3+</sup> stable in the mantle component of the lid to enable polaron coupled 'fast' diffusion of H<sup>+</sup> appears reasonable. Most likely, however, H<sup>+</sup> diffusion will proceed by simultaneous fast diffusion coupled to flux of polarons, and 'slow' diffusion coupled to diffusion of metal cation vacancies within olivine. Therefore, data from Padron-Navarta et al. (2014) on H<sup>+</sup> diffusivity in Fe-free forsterite, coupled to slower diffusion of metal vacancies, was also used to constrain slow diffusion of H in olivine.

Diffusion of H<sup>+</sup> in orthopyroxene can also proceed via a fast mechanism coupled with Fe redox change, and a slower mechanism coupled to diffusion of metal vacancies. To model

both processes experimental diffusivity data of Stalder et al. (2007), Stalder and Behrens (2006), and Stalder and Skogby (2003) was used. In contrast to the limited studies on orthopyroxene, there have been numerous, sometimes conflicting studies of H<sup>+</sup> diffusion in clinopyroxene. Differences between studies are most likely due to the more complex crystal chemistry of clinopyroxene. For fast, redox coupled diffusion, data from Ferriss et al. (2016) for H<sup>+</sup> diffusivity in clinopyroxene from Nushan was used, which is, according to Ferriss et al. (2016), most comparable to mantle clinopyroxene. Slow diffusion in clinopyroxene was modelled using data on H<sup>+</sup> diffusivity in Fe-free diopside from Sundvall et al. (2009). In contrast to other phases, H<sup>+</sup> diffusion in plagioclase is relatively anisotropic, and there is no evidence for fast redox driven diffusion. Diffusion was modelled using data from Johnson and Rossman (2013), who determined H<sup>+</sup> diffusivity in plagioclase coupled to Na<sup>+</sup> diffusion.

In a polycrystalline material, species can diffuse through crystal structures (bulk, or lattice diffusion), or through grain boundary regions. Diffusivity in grain boundary regions is typically faster, although the low volume fraction of grain boundary regions in most systems means that lattice diffusion typically dominates, except in very fine grained material and/or at lower temperatures. Demouchy (2010a) and Hiscock (2012) demonstrated that H<sup>+</sup> grain boundary diffusion in olivine may contribute towards total flux of H<sup>+</sup> in Earth's mantle under certain conditions. In the absence of data on H<sup>+</sup> grain boundary diffusion for other silicates, we use data from Demouchy (2010a) to model grain boundary H<sup>+</sup> flux in the stagnant lid. Given mineral proportions within mantle lithologies it is likely that this approach provides a good estimate of the contribution of grain boundary diffusion of H<sup>+</sup>. To model the contributions of both lattice and grain boundary diffusion within the lid we use, in accordance with Demouchy (2010a), the following equation (Balluffi et al., 2005):

$$D_H^{eff} = D_H^L + \left(\frac{3\delta}{d}\right) \cdot D_H^{gb} \quad [1]$$

where  $D_H^{eff}$  is effective (i.e. total) H diffusivity,  $D_H^L$  and  $D_H^{gb}$  are lattice and grain boundary H diffusivities, respectively,  $d$  is grain size and  $\delta$  is grain boundary width. Effective  $H^+$  diffusivity in the lid is, therefore, determined based on a weighted average of diffusivities in crystal lattice and grain boundary regions, without accounting for the likely segregation of  $H^+$  into grain boundary regions. This, coupled with faster grain boundary diffusivity, might result in slightly higher effective diffusivity. Grain size for [1] is set in the model for both regions of the model stagnant lid. A representative grain boundary width of 0.75 nm, consistent with previous studies (Bromiley and Hiscock, 2016; Demouchy, 2010b, 2010a), is assumed.

A single value of  $D_H^L$  was used for each shell of the model, determined by first calculating an average diffusivity for H in each phase, and then weighting this based on mineral proportions. H diffusivity in most mineral structures is typically highly anisotropic. In olivine, for example, H diffusivity parallel to the crystallographic  $a$  axis is approximately one order of magnitude faster than diffusivity parallel to the  $b$  and  $c$  axes. To test the validity of using an average (i.e. bulk) H diffusivity, I calculated average diffusivity in one direction for a system of 1000 randomly oriented grains, assuming various order of magnitude differences in diffusivity in 2 orthogonal directions. Even in a system where there is a 2 order of magnitude difference in diffusivity in 2 orthogonal directions, average (mean) diffusivity gives, within error, the same result as the actual average diffusivity for 1000 grains (calculated for each individual grain based on actual orientation relative to the 2 orthogonal directions). Therefore, for a sufficient large number of randomly oriented grains, an average diffusivity can be assumed based on the weighted average of diffusivities in different crystallographic orientations.

Figure 2 shows how bulk  $D_{eff}^H$  for each shell changes as a function of depth for 4 model temperature profiles, calculated assuming fast, polaron coupled H diffusion (also see supplementary online material). Temperature profiles are described in detail below, and are

based on proposed models for Venus or a Venus-like planet. Modelling demonstrates that temperature has a dominant influence on  $D_{eff}^H$ , which in turn decreases markedly upwards into the lid as a function of the temperature profile. As diffusivity decreases upwards into the lid, diffusion will eventually cease to be effective over geological timescales. H flux will effectively stagnate at some distance into the lid, implying that only the lowermost portions of the lid can become hydrated. Figure 2 also demonstrates that H diffusivity varies markedly with small variations in temperature over conditions at the base of the lid.

To determine the extent of H flux into the lid, diffusion was modelled over discrete time intervals using a standard infinite source solution to Fick's second law, based on  $D_H^{eff}$  calculated from [1]:

$$C(x, t) = C_S - (C_S - C_0) \operatorname{erf} \left[ \frac{x}{2\sqrt{D_H^{eff} t}} \right] \cdot C_S \quad [2]$$

where  $C(x, t)$  is the concentration of the diffusing species, after time  $t$  at a given distance  $x$  from the source. Within the model, each 10 km shell was further divided into 100m slices. The source for each slice in the model represents the lower boundary of the slice (see below), and  $C_S$  and  $C_0$  are the concentrations of the diffusing species in the source (the convecting mantle or underlying slice) and the sink (the slice) prior to diffusion.

### **2.3 Diffusivity of other species**

Given that there is no evidence for even ppm concentrations of C in mantle minerals, effectively limiting any influence of lattice diffusion, C flux was modelled solely based on data from Hayden and Watson (2008) on grain boundary diffusivity of C in polycrystalline olivine, again using [1] and [2]. Although the data of Hayden and Watson (2008) only allow the total

effective diffusivity of C in grain boundary regions to be ascertained, it is assumed that this represents diffusion of atomic C. A similar approach to that outlined for H was used to model diffusion of Ar and He. Data from Thomas et al. (2008) and Cassata et al. (2011) was used to determine Ar diffusivity in olivine and pyroxene, respectively. He diffusivity in olivine and pyroxene was modelled using data from Tolstikhin et al. (2010) and Trull (1981), respectively, and grain boundary diffusion of both noble gases modelled using data from Burnard et al. (2015).

#### **2.4 Modelling diffusion through the model stagnant lid**

The model stagnant lid used here is constructed of a stacked vertical sequence of 100m thick slices. The bottom surface of the first slice ( $S_1$ ) corresponds to the base of the stagnant lid ( $D_1$ ), at a depth of 170km from the surface. The top surface of this first slice is at a depth of  $D_1-2i$ , where  $i=1000\text{m}$ . The next (second) slice in the model then has boundaries at  $D_1-i$  and  $D_1-3i$ ; as such, there is a 50% overlap between the slices, as shown in figure 3. The remainder of the model consists of an upward sequence of similarly overlapping slices. Average temperature for each slice is set using data shown in figure 2..

Diffusion through this sequence of overlapping slices was modelled over a series of time steps. The initial conditions for the model have an element concentration at  $D_1$  of  $X_0$  ppm (figure 2A). This corresponds to the element concentration in the underlying convecting mantle (i.e. the infinite source,  $C_s$ ) which remains constant throughout each subsequent time step. Element concentration at  $D_1-2i$  (corresponding to  $C_0$  in [2]) is typically set at 0 ppm for most modelling here, to represent an anhydrous stagnant lid. For time step 1, [2] is then used to model diffusion of the species over a given time interval, at distances of 100 m, to produce a concentration gradient. Representative input and output from this single time step are shown in figure 3A,B.

The second time step uses the output of time step 1 as input data. For slice one,  $C_0$  is set across the shell, at 100m intervals, based on the output for this slice from time step 1. Element concentration at  $D_1$  remains constant. For slice 2, from  $D_{1-i}$  to  $D_{1-2i}$ , input from time step 1 gives an initial element concentration. The duration of the time step used throughout the modelling is chosen so that the element concentration at  $D_{1-2i}$  approaches  $C_0$  (typically 0). Element concentration from  $D_{1-2i}$  to  $D_{1-3i}$  is then set at  $C_0$ . For slice 2, the initial concentration from  $D_{1-i}$  is used for  $C_s$  in [2]. Diffusion across both slices is then modelled using [2], and concentration profiles recorded, as shown in figure 2C,D. Output from this time step is then used as the input for time step 3, over which diffusion is modelled for slice 1 to 3 (figure 2E). Thus, step wise modelling is used to simulate diffusion with increasing time across the stagnant lid. Using this approach, flux across the entire stagnant lid, where diffusivity changes as a function of distance, can be modelled. The step size (slice size) and time step are chosen to ensure that during each step diffusion of the species can be fully modelled within the shell; as such, progressive diffusion across consecutive slices is modelled step-wise, and flux approximated.

### **3. *Fast H diffusion, Nimmo and McKenzie (1998) model.***

Diffusivity of H is strongly temperature dependent, and the relative importance of diffusion as a mechanism for mobilising H will depend on the temperature profile across the stagnant lid. Venus potentially provides a useful model for an Earth-like planet with a stagnant lid regime, aside from arguments regarding episodic overturn. However, the geothermal gradient on Venus has not been determined. Here, we use proposed temperature profiles from previous studies to input into the model. Nimmo and McKenzie (1998) proposed a temperature structure for Venus based on a mantle potential temperature similar to that of the Earth, 1573K (figure 3A), a 170 km thick stagnant lid, mechanical boundary layer thickness constrained by melt generation and admittance, inferred viscosity and surface temperature of 723 K (figure 2). This temperature profile is close to a geothermal gradient on Venus of 6 K/km (figure 2), and would be consistent with a stable mantle structure in which melting

could only occur as a result of significant temperature fluctuations (i.e. thermal plumes) or, by analogy to the Earth, by large scale tectonic processes such as rifting and lithospheric thinning. Here, we use the Nimmo and McKenzie (1998) temperature structure to constrain convecting mantle-lid interaction in a system where the deep interior is not degassed. A mantle H content equivalent to 1000 ppm H<sub>2</sub>O by weight was used. By comparison, the uppermost terrestrial mantle (the source region for mid-ocean ridge basalts) is estimated to contain up to 200 ppm H<sub>2</sub>O based on various geochemical arguments (Peslier, 2010). However, it is likely that the water content of Earth's mantle is highly variable, both due to systematic variations in H storage capacity with depth (Bolfan-Casanova, 2005; Smyth et al., 2006) and as a result of large scale plate movement. The uppermost mantle of Earth has been depleted by both formation of continental crust and large scale mantle melting at divergent plate margins, so likely does not give meaningful insight into the bulk H content of the silicate Earth. The mantle source region for ocean island basalts (i.e. plume related mantle melting) is considerably more H-rich, containing up to 1000 ppm H<sub>2</sub>O, for example (Peslier, 2010). The deeper terrestrial mantle may be more H-rich than this due to a marked increase in H storage capacity as a function of pressure and changes in mantle mineralogy (e.g. Bolfan-Casanova, 2005; Bolfan-Casanova et al., 2000).

Figure 4 shows the results of modelling H diffusion based on the Nimmo and McKenzie (1998) profile, with H concentration gradients shown after  $t = 100$  Myr, 200 Myr, 500 Myr, 1 Gyr and 2 Gyr, from right to left. Concentration profiles arising due to H diffusion through the model lid have a characteristic S-shaped form. From left to right in figure 4, with increasing depth, the first change in gradient in each profile represents the maximum distance to which H can diffuse after a given period of time, or the diffusive front ( $D_F$ ). Each profile then has a relatively constant gradient, the steepness of which is a function of how quickly bulk modelled diffusivity changes with depth/temperature. The concentration gradient then rapidly decreases as the profile levels out to approach the H content of the convecting mantle. This



distance can be defined as the saturation front ( $S_F$ ) as it represents the distance at which a given portion of the lid, after time  $t$ , attains the maximum volatile content possible via diffusion.

The extent of H diffusion using this temperature profile is limited. After 2 Gyr,  $S_F$  extends only 5.5 km into the base of the lid, with  $D_F$  extending to around 35 km. H concentration profiles are relatively steep as temperature, and thus diffusivity, drops markedly with distance upwards into the lid (Figure 2). The water storage capacity of the lid, or the maximum solubility of  $H_2O$  in the 2 phase olivine + orthopyroxene mix, indicated on figure 4 is based on pressure/temperature dependence of H solubility summarised in Bolfan-Casanova (2005). Water storage capacity of the base of the lid is >1700 ppmw  $H_2O$ , and decreases with increasing distance into the lid due to a decrease in H solubility in both olivine and orthopyroxene with decreasing pressure. Water storage capacity only approaches 1000 ppmw  $H_2O$  around 50 km into the lid; as such, all H diffusing into the lid can be fully incorporated as interstitial defects within olivine and orthopyroxene, with no additional hydrous phase present. This would also be the case for a more complex stagnant lid mineralogy containing additional clinopyroxene  $\pm$  garnet (i.e. more lherzolitic composition).

For comparison with the model presented here, the light grey line in Figure 4 shows a concentration gradient calculated for a single 'infinite source' solution to Fick's second law, for a comparable time period of 2 Gyr. This is calculated assuming a convecting mantle water content of 1000 ppmw  $H_2O$ , a fixed boundary between convecting mantle and anhydrous lid, and a single  $D_H^{eff}$  across the entire lid, based on the value for the lowermost shell. As expected, there is a marked difference in gradient compared to outputs from the model where  $D_H^{eff}$  decreases markedly upwards through the lid. H diffuses a much greater distance into the lid, which is only effectively saturated at the boundary with the convecting

mantle. As a consequence, distribution of H across the lowermost lid varies considerably, and in marked contrast to the model presented here. However, a simple calculated characteristic diffusion distance,  $L_D = \sqrt{D_H^{eff} \cdot t}$  does give a reasonable insight into the extent of H flux in the model. For example, a constant  $D_H^{eff} \approx 10^{-8} \text{ m}^2 \cdot \text{s}^{-1}$  (Figure 2) implies  $L_D \approx 18 \text{ km}$  after 1 Gyr, and  $\approx 25 \text{ km}$  after 2 Gyr, which compares reasonably well with the extent of migration of concentration profiles over the same time intervals.

The thin grey line in figure 4 marks the solidus for harzburgite determined by Maaloe (2004). Harzburgite is, terrestrially, a melt residue formed by large degree (typically 15-25%) melting of garnet lherzolite. As such, it is not surprising that the solidus for harzburgite greatly exceeds temperatures across the lid. Harzburgite composition was used for diffusion modelling in this study as it represents a simple mantle composition from which basaltic melt has been extracted. However, it is also broadly representative of any ultramafic (i.e. olivine dominate) peridotitic composition. Exact mineralogy of any stagnant lid will depend on the complexity of geological processes which it has been subjected to, and the bulk silicate composition of the planet. A more generic peridotitic composition, under conditions of the lower portion of the stagnant lid, would likely additionally comprise garnet and clinopyroxene. The presence of these decreases the mantle solidus markedly, although would have only a very minor influence on bulk H diffusivity. Dashed lines on figure 4 mark positions of a dry (i.e. H-free) peridotite solidus, and solidi for peridotite with 200 ppmw and 1000 ppmw  $\text{H}_2\text{O}$ , respectively, as determined by thermodynamic modelling of the effect of H incorporation on depression of the mantle solidus (Hirschmann, 2006). A nominal 'wet' mantle solidus lies  $>200 \text{ K}$  lower than the harzburgite solidus, depending on the exact water content. However, from figure 4 it is apparent that all mantle solidi are substantially ( $>100\text{K}$ ) higher than lid temperatures across the model. As such, diffusion of H into the lid in this model is unable to induce partial melting. For a constant temperature profile across a stable lid over Gyr timescales diffusion will, however, depress the solidus of the lower 10-20 km portion of the

lid by approximately 50-100K, due to the presence of 200 ppm-1000 ppmw H<sub>2</sub>O. This will significantly increase the likelihood of 'wet' melting of the base of the lid due to thermal anomalies such as upwelling plumes. The extent of wet melting will be a function of the lifetime of the stagnant lid, and the H content of the convecting mantle. However, in the general case where a less degassed interior is overlain by a relatively anhydrous stagnant lid, diffusion of H increases the possibility that upwelling plumes promote melting, and rejuvenation, of the lowermost portion of the lid in Venus, and exo-Venus planets.

In terms of loss of water from the convecting mantle to the stagnant lid, diffusion modelling indicates that  $4 \times 10^{18}$  kg are transferred to the stagnant lid after 10 Myr, increasing to  $2 \times 10^{19}$  kg after 1 Gyr and  $3 \times 10^{19}$  after 2 Gyr. If we assume, in crude comparison to the Earth, that water in the mantle of Venus is distributed over the upper mantle and mantle transition zone, this equates to a loss of mantle water content to the lid of between 0.0005 and 0.0034%. As such, loss of water from the mantle to the lid by diffusion is inconsequential. Any diffusive loss of H will have no impact on mantle properties, and make no effective contribution to mantle degassing. In this regard, the lid acts as a relatively impermeable barrier to volatile loss and interior/atmospheric exchange.

#### **4. Slow H diffusion and flux of other species, Nimmo and McKenzie (1998) model**

Figure 5 shows a comparison of concentration profiles for different species after 2 Gyr using the same Venusian temperature profile from Nimmo and McKenzie (1998). Even after a protracted period of 2 Gyr, slow diffusion of H, i.e. coupled to metal vacancies as opposed to Fe redox changes, only results in a  $D_F$  extending under 2 km into the lid. As expected, therefore, diffusion mechanism has a significant control on the effectiveness of diffusive loss of H to the stagnant lid. For reduced stagnant lids, H diffusion will be largely coupled to slower metal vacancy diffusion, and the extent of H mobility is limited, even over Gyr timescales. However, in larger stagnant lid regime planets, mantle self-oxidation during

magma ocean crystallisation should occur as a consequence of mantle crystallisation (Frost et al., 2004; Frost and McCammon, 2008). Furthermore, operation of redox pump type mechanisms, as inferred for Venus, might also further promote mantle oxidation. This will promote fast H diffusion due to the presence of  $\text{Fe}^{3+}$  in olivine and pyroxene within NAMs in the lid, and much greater flux of H.

Diffusion of other volatiles is also extremely limited. As shown in figure 5,  $D_F$  for He and Ar are approximately 2 km and <0.5 km, respectively. Little effective diffusion of C occurs in the model as flux is only possible through grain boundaries. The limited data available on volatile diffusivities for these species in the various mantle phases, and within grain boundaries, and large potential variability in the proportion of grain boundaries within the model lid (which is a function of grain size and grain boundary width) mean that modelled concentration gradients in Figure 5 have a significant error on them. However, they are broadly illustrative, and imply that diffusion of all volatile species other than H, when not coupled to flux of metal vacancies, is inconsequential. As expected, solid state diffusion can only result in effective mobilisation of H in stagnant lid regime planets, unless mantle temperatures greatly exceed those expected in Venus-like planets.

## **5. Fast H diffusion, Ghail (2015) model**

Ghail (2015) proposed a model for Venus where the presence of  $\text{CO}_2$  in the mantle results in minor melting and the formation of an asthenosphere. In this model, plume activity results in lid rejuvenation, which significantly contributes to heat loss and allows Venus to maintain a stable tectonic regime. Ghail (2015) suggested that the  $12 \text{ mWm}^{-2}$  geotherm shown in Figure 2 can be used to approximate the temperature profile through a region of old, stable lid on Venus, i.e. a cool lid unaffected by plume activity. Over the lowermost lid this temperature profile is somewhat similar to a  $5 \text{ K/km}$  geothermal gradient (figure 2). The  $18 \text{ mWm}^{-2}$  geotherm approximates, according to Ghail (2015) the thermal structure of a region of the lid

heated by a mature plume, but at a distance from the plume tail. He further proposed that a 36 mWm<sup>-2</sup> geotherm approximates the thermal structure of a region of the lid directly heated by an impinging plume head. Therefore, these proposed geotherms provide an alternative thermal structure for Venus which can be used to assess the extent of volatile flux through an old, stable lid, and also a hotter lid heated by plume activity. Figure 6 shows these modelled Venusian geotherms and melt relations from Falloon and Green (1989) for the corresponding carbonated peridotite mantle composition. Ghail (2015) suggested that intersection of 18 and 36 mWm<sup>-2</sup> geotherms with 'minor' and 'major' melting curves (i.e. mantle solidi) results in small to large degrees of melting towards the base of a CO<sub>2</sub>-bearing peridotitic Venusian stagnant lid heated by upwelling plumes.

H concentration profiles shown in Figure 6 are based on temperature profiles consistent with 18 and 12 mWm<sup>-2</sup> geotherms, for the same 5 times steps shown in Figure 4. A 12 mWm<sup>-2</sup> geotherm infers temperatures <1600K across the lowermost stagnant lid. This reduces the extent of H diffusion, and concentration profiles in figure 6B show that D<sub>F</sub> progresses <30km into the lid after 2 Gyr, and just over 20 km after 1 Gyr. Once again, temperatures across hydrated regions of the lid are sufficiently below than the lid solidus for H to have any influence on lid stability. This temperature profile, similar to that derived from Nimmo and McKenzie (1998) again suggests that H flux into an old stagnant lid is relatively minor, only partially hydrated the lowermost portions of the lid.

The 18 mWm<sup>-2</sup> geotherm can be used to approximate temperature profile through a region of the lid heated by plume activity, but not directly involved in plume upwelling and mantle melting. Figure 6A demonstrates that higher temperatures across the lowermost lid, and a flatter temperature profile greatly enhance H flux and change the shape of H concentration gradients. A difference in the shape of H concentration gradients between figures 6B and 6A and figure 4 highlight the effect that a drop in temperature upwards through the lid has in

stalling H diffusion. For flatter temperature profiles, H concentration profiles have a lower gradient, and the difference between  $D_F$  and  $S_F$  remains large. For typical sloping temperature profiles, where diffusivity drops markedly with distance into the lid, H concentration profile gradients are steeper, and H flux reduces with time/distance. This means that, regardless of the increasing effects of evolution in lid temperature with time or lid stability, forward modelling H diffusion for periods of time exceeding 2 Gyr is of limited value for most geotherms: the extent of additional migration of both the  $S_F$  and  $D_F$  will be limited. For the Ghail (2015)  $18 \text{ mWm}^{-2}$  geotherm, there is a greater separation of the  $S_F$  and  $D_F$  even at considerable distance into the lid. After 2 Gyr,  $D_F$  extends to nearly 50 km upwards into the lid, with  $S_F$  extending upwards approximately 25 km. However, a change in the 2 Gyr H concentration profile around 125 km depth indicates that the continual, small drop in temperature and concurrent drop in diffusivity, as shown in Figure 2, start to result in stagnation in H flux, which would with time result in steepening of the H concentration gradient. Importantly, this stagnant occurs over the range of depths where there is only a small decrease in temperature, highlighting the fact that small changes in inferred temperature control whether solid state diffusion is relevant.

Timescales used for the modelling shown in figure 6A obviously exceed the duration of localised heating from a plume, which is presumably stable on 100 Myr time scales at most, and ignore any localised lid instability due to plume activity (Davaille et al., 2017). Lid temperature would be expected to slowly drop after cessation of adjacent upwelling. Similarly, for a slowly heating stagnant lid regime planet (Venus, or Venus analogue, hybrid stagnant lid regime), 1 Gyr probably approaches or exceeds the time period of temperature fluctuations between episodes of large scale melting and resurfacing (Rolf et al., 2017). Comparison of profiles in figures 6A and 6B can, however, be used to assess the effect of temperature changes on H flux into the lid. The grey shaded region shown in Figure 6B is delimited by H concentration profiles after 2 Gyr for both  $12 \text{ mWm}^{-2}$  and  $18 \text{ mWm}^{-2}$  geotherms. This

depth-concentration space provides constraints on the effect of temporal heating of the base on the stagnant lid within the Ghail (2015) model.

The difference between calculated water-depressed mantle solidi and the carbonated peridotite melting relations shown in figure 6 is due to phase stability and total volatile content contrast in the two systems: i.e. trace amounts of water for peridotitic solidi vs 2.4 wt% CO<sub>2</sub> in a carbonated peridotite. The 18 and 36 mWm<sup>-2</sup> geotherms intersect the +1000ppm H<sub>2</sub>O mantle solidus at around 125 km depth, and the +200 ppmw H<sub>2</sub>O solidus around 95 km depth. As such, diffusion is unable to deliver H far enough into the lid to induce lid melting. For example, the maximum distance into the lid to which 200 ppmw H<sub>2</sub>O can diffuse in the model corresponds to a depth just over 125 km, even after 2 Gyr for a lid continually heated by plume activity. However, in a Ghail (2015) type model, where plume activity promotes melting and lid rejuvenation, diffusion does result in significant transport of H into lower portions of the lid. Melt relations under these conditions for carbonated peridotite are poorly constrained. However, a period of 100 Myr is sufficient, with an elevated mantle geotherm, to promote diffusion of around 200 ppmw H<sub>2</sub>O 5 km into the lid. This distance exceeds 15 km after 500 Myr, 25 km after 1 Gyr, and 43 km after 2 Gyr. As such, for a stable planet within the stagnant lid regime, diffusion will result in a hydrated lowermost lid. In a regime where melting is promoted by the presence of CO<sub>2</sub>, the presence of water would increase the degree of melting, modify melt relations and melt chemistry, and further enhance lid rejuvenation.

The Ghail (2015) model assumes that the mantle component of the lid contains CO<sub>2</sub> in significant enough proportions to considerably depress the solidus. In contrast, the starting point for diffusion modelling here is an anhydrous lid. The effect of an H-bearing lid can be readily simulated by setting C<sub>0</sub> in [2] to any given value. In figure 6C, concentration profiles based on a Ghail 18mWm<sup>-2</sup> geotherm are shown for an anhydrous lid, and convecting

mantle with 1000 ppmw H<sub>2</sub>O, and a lid with a uniform 200 ppmw H<sub>2</sub>O. By definition, varying C<sub>S</sub> has no influence on D<sub>F</sub> or S<sub>F</sub> except where C<sub>0</sub> approaches C<sub>S</sub>. However, for any given time, the distance to which water concentrations intermediate between C<sub>0</sub> and C<sub>S</sub> extend into the lid is increased slightly, increasing the possibility of water-induced partial melting.

## **6. Fast diffusion in a hot stagnant lid: assessing the importance of H diffusion**

From concentration profiles shown in figures 6A it is clear that slightly higher temperatures at the base of the lid using a Ghail 18 mWm<sup>-2</sup> geotherm, and a relatively flat geotherm over the lower portions of the lid, result in significantly enhanced H flux. To fully explore the extent of H diffusion, a ‘hot exo-Venus’ temperature profile was used assuming (1) a wet (1000 ppmw H<sub>2</sub>O), broadly peridotitic convecting mantle and olivine-rich lid, (2) a temperature at the top of the convecting mantle just below the 1000 ppmw H<sub>2</sub>O solidus, and (3) a surface T of 723 K. Within the bounds of the model this profile represents the hottest the base of the stagnant lid can be before the onset of partial melting, for an approximately terrestrial mantle composition. As shown in Figure 2, it lies between 6 and 7 K/km geothermal gradients.

The continual temperature reduction upwards through the stagnant lid with this profile results in a sharp decrease in H diffusivity (Figure 2), ultimately producing steeper H concentration gradients, as shown in figure 7. However, the effect of elevated temperatures relative to other profiles is to increase H flux significantly. After 2 Gyr, D<sub>F</sub> moves ~45 km into the lid (~15, 25, 33, and 40 km after 100 Myr, 250 Myr, 500 Myr and 1 Gyr, respectively). More importantly, S<sub>F</sub> also progresses significantly into the lid, resulting in H<sub>2</sub>O contents of around 1000 ppmw ~30 km into the lid after 2 Gyr, ~20 km after 1 Gyr and ~10 km after 500 Myr. Due to starting conditions in this model the geotherm never intersects the 1000 ppmw H<sub>2</sub>O, and because water contents remain below the storage capacity, diffusion cannot induce melting or stabilise a free fluid phase. For this to occur H would need to diffuse 60 km or



more into the lid, which, given that diffusivity is reduced markedly upwards, cannot feasibly occur due to stagnation in H flux. Within this static model, therefore, regardless of the T profile across the lid, diffusion of H will never induce lid melting on its own. The effect of any progressive increase in temperature, i.e. for a stagnant lid regime planet slowly heating prior to eventual lid overturn and a planetary resurfacing event, will instead be to initially induce melting in the deeper convecting mantle. However, H diffusion can play an important role in terms of H redistribution across the convecting mantle and lid. From figure 7 it is evident that a slightly increased ambient mantle temperature results in hydration of the lowermost lid; comparison with figure 4 highlights the dominant influence that temperatures across the bottom of the lid have on the extent of  $S_F$  and  $D_F$  migration. For Venus, temperature profiles remain, due to a lack of primary data, very poorly unconstrained. For other stagnant lid planets, temperature profiles through the lid and the uppermost convecting mantle will define the importance of H diffusion into the lid. If we assume that stagnant lid regimes are stable up to 0.5 Gyr or longer, in between or in the absence of periods of global resurfacing, Venus sized or larger hot exoplanets can be envisaged as having slightly ‘leaky’ stagnant lids. Diffusion results in equilibration of H contents across the convecting mantle and lowermost lid to distances of 10s of km or greater. Whilst this does not promote melting within the lid, it does have the effect of significantly lowering the lid solidus, such that any thermal perturbations, for example upwelling plumes, are much more likely to result in localised lid melting.

## **7. The importance of H diffusion and limitations in the model**

Whether H diffusion and lid hydration is important depends both on the temperature profile across the lowermost lid in stagnant-lid regime planets, and lid stability. The temperature profile across the Venusian mantle remains poorly constrained, and given the paucity of data, a slightly hotter Venusian mantle is certainly not impossible. Higher mantle temperatures will certainly occur in a given proportion of exo-Venus planets. It is also likely

that the interior of Venus was hotter earlier in the history of the planet and/or that Venus undergoes periods of periodical heating and eventual global melting. As noted by Ghail (2015), mechanisms which promote lid rejuvenation are of use in explaining heat flow in stagnant lid regimes, which is otherwise much less efficient than with plate tectonics. It is important to note, however, that modelling here is based on a number of simplified assumptions. The lid is modelled as having a hazburgitic composition. This gives a reasonable assessment of bulk H mobility in various systems, as H diffusivities in peridotitic mineral assemblages, which are similarly olivine-dominant, will not be significantly different. Much less certain remains mantle melt relations which are highly composition dependent, and vary significantly with major element and volatile content. For a truly hazburgitic mantle lid, melting is not expected to occur even in the presence of considerable H<sub>2</sub>O. However, such a lid composition is unrealistic; the solidus for more peridotitic compositions is considerably lower, implying that H can have a variable influence on lid stability, but only after geotherms are locally elevated by upwelling plumes. Likewise, for other bulk silicate planetary compositions, mantle potential temperatures, and the extent of H flux, could be significantly higher whilst lids remain stable. However, temperature gradients across the mantle will also control thickness of the stagnant lid, so any assessment of H flux in hot stagnant lid planets would require a detailed modelling of planetary evolution.

The starting distribution of volatiles in the model used is based on extreme convecting mantle-lid fractionation, with a volatile-rich interior and anhydrous lid. More likely, lowermost portions of the lid would incorporate some H, unless they represented true melt residue from which volatiles were stripped, or regions of the mantle affected by previous melt processes. However, the presence of pre-existing H in the lid does not influence H diffusion significantly, as the effect of decreasing T upwards into the lid means that H flux stagnates, and the maximum H content of the lid is always limited by H content in the convecting mantle. Importantly, for the model presented here, regardless of lid H content and T profile, H

diffusion can never result in overstepping of a realistic 'wet' or 'damp' solidus, and melting will always be initiated in the underlying convecting mantle.

The model developed here is static and assumes that the temperature profile through the lid does not vary with time. It also assumes that the lid is stable and does not vary in thickness or become altered by any geological process. This simplification allows varying diffusivity across a complex geomaterial to be modelled, and importantly, the considerable influence of varying temperature of volatile mobility to be assessed. Thermal structures of planets, however, obviously vary significantly with time. The stagnant lid is itself the result of thermal evolution of the entire planet, and represents a thermal boundary layer across which heat is conducted from the convecting mantle to the surface. A more accurate assessment of H flux would require a time-dependent model of the lid, including evolution of convecting mantle temperature, of lid temperature and thickness, and also of crust thickness (Rolf et al., 2018). However, the fact that diffusivities vary considerably with even small changes in temperature would greatly add to the complexity of such a model, as would the fact that the presence of H, and variations in H concentration, in turn have a disproportionate influence on physical properties, notably both rheology and thermal stability (e.g. Peslier, 2010). Furthermore, a more accurate assessment of the extent of H diffusion would require a more accurate initial H distribution across the model. This distribution is dependent on factors such as magma ocean crystallisation, which remain poorly constrained.

Results here suggest, within the limitations of a static model with simple imposed H concentration gradient, that conditions towards the base of a model Venusian stagnant lid are transitional between solid state diffusion effectively redistributing H and having no meaningful effect. Aside from considerable uncertainties regarding the internal structure of Venus and temperature profile through the lid it should also be noted that H diffusivities over temperatures expected at the base of the lid are based on experimental data at considerably

lower temperatures (typically <1473 K for data used here). Diffusion laws for H in mantle minerals are also variably constrained, adding to uncertainties in extrapolated H diffusivities. Any appreciable H flux is insignificant in terms of volatile flux from the convecting mantle, although its effect of mantle solidus would be to promote lid rejuvenation, for example during plume heating. For exoplanets with higher temperatures across the stagnant lid, H diffusivity is markedly increased, resulting in considerable H flux over 100 Myr timescales. Mature stagnant lids in hotter, exoVenus planets can be envisioned as ‘slightly leaky’ in terms of H, with diffusion destabilising the lowermost lid by reducing the mantle solidus. Given the importance of H in terms of mantle properties ranging from melting behaviour to rheology, future models of such planets should assess the effects of solid state diffusion of H.

## **Acknowledgements**

The author thanks an anonymous reviewer and Dr Sami Mikhail, whose comments and suggestions improved this manuscript considerably.

## References

- Airey, M.W., Mather, T.A., Pyle, D.M., Glaze, L.S., Ghail, R.C., Wilson, C.F., 2015. Explosive volcanic activity on Venus: The roles of volatile contribution, degassing, and external environment. *Planet. Space Sci.* 113, 33–48. <https://doi.org/10.1016/j.pss.2015.01.009>
- Altwegg, K., Balsiger, H., Bar-Nun, A., Berthelier, J.J., Bieler, A., Bochsler, P., Briois, C., Calmonte, U., Combi, M., De Keyser, J., Eberhardt, P., Fiethe, B., Fuselier, S., Gasc, S., Gombosi, T.I., Hansen, K.C., Haessig, M., Jaeckel, A., Kopp, E., Korth, A., Leroy, L., Mall, U., Marty, B., Mousis, O., Neefs, E., Owen, T., Reme, H., Rubin, M., Semon, T., Tzou, C.-Y., Waite, H., Wurz, P., 2015. 67P/Churyumov-Gerasimenko, a Jupiter family comet with a high D/H ratio. *Science*. 347 (6220) article no. 1261952 <https://doi.org/10.1126/science.1261952>
- Angelo, I., Rowe, J.F., Howell, S.B., Quintana, E. V, Still, M., Mann, A.W., Burningham, B., Barclay, T., Ciardi, D.R., Huber, D., Kane, S.R., 2017. Kepler-1649b: An Exo-Venus in the Solar Neighborhood. *Astron. J.* 153. <https://doi.org/10.3847/1538-3881/aa615f>
- Balluffi, R.W., Allen, S.M., Carter, W.C., 2005. *Kinetics of Materials*. Blackwell Science Publ (Oxford, England). 645p.
- Barstow, J.K., Aigrain, S., Irwin, P.G.J., Kendrew, S., Fletcher, L.N., 2016. Telling twins apart: exo-Earths and Venuses with transit spectroscopy. *Mon. Not. R. Astron. Soc.* 458, 2657–2666. <https://doi.org/10.1093/mnras/stw489>
- Bell, D.R., Rossman, G.R., 1992. Water in Earth's Mantle. The role of nominally anhydrous minerals. *Science*. 255, 1391–1397.
- Bertaux, J.-L., Vandaele, A.-C., Korabiev, O., Villard, E., Fedorova, A., Fussen, D., Quemerais, E., Belyaev, D., Mahieux, A., Montmessin, F., Muller, C., Neefs, E., Nevejans, D., Wilquet, V., Dubois, J.P., Hauchecorne, A., Stepanov, A., Vinogradov, I., Rodin, A., Team, S.S., 2007. A warm layer in Venus' cryosphere and high-altitude measurements of HF, HCl, H<sub>2</sub>O and HDO. *Nature* 450, 646–649. <https://doi.org/10.1038/nature05974>

744 Bezard, B., Tsang, C.C.C., Carlson, R.W., Piccioni, G., Marcq, E., Drossart, P., 2009. Water  
 745 vapor abundance near the surface of Venus from Venus Express/VIRTIS observations.  
 746 J. Geophys. Res. 114. E00B39. <https://doi.org/10.1029/2008JE003251>  
 747 Bolfan-Casanova, N., 2005. Water in the Earth's mantle. Mineral. Mag. 69, 229–257.  
 748 <https://doi.org/10.1180/0026461056930248>  
 749 Bolfan-Casanova, N., Keppler, H., Rubie, D.C., 2000. Water partitioning between nominally  
 750 anhydrous minerals in the MgO-SiO<sub>2</sub>-H<sub>2</sub>O system up to 24 GPa: implications for the  
 751 distribution of water in the Earth's mantle. Earth Planet. Sci. Lett. 182, 209–221.  
 752 Bromiley, G.D., Hiscock, M., 2016. Grain boundary diffusion of titanium in polycrystalline  
 753 quartz and its implications for titanium in quartz (TitaniQ) geothermobarometry.  
 754 Geochim. Cosmochim. Acta 178, 281–290. <https://doi.org/10.1016/j.gca.2016.01.024>  
 755 Bromiley, G.D., Keppler, H., 2004. An experimental investigation of hydroxyl solubility in  
 756 jadeite and Na-rich pyroxenes. Contrib. to Mineral. Petrol. 147, 189–200.  
 757 Bromiley, G.D., Keppler, H., McCammon, C.A., Bromiley, F.A., Jacobsen, S.D., 2004.  
 758 Hydrogen solubility and speciation in natural, gem-quality Cr-diopside. Am. Mineral. 89,  
 759 941–949.  
 760 Burnard, P.G., Demouchy, S., Delon, R., Arnaud, N.O., Marrocchi, Y., Cordier, P., Addad,  
 761 A., 2015. The role of grain boundaries in the storage and transport of noble gases in the  
 762 mantle. Earth Planet. Sci. Lett. 430, 260–270.  
 763 <https://doi.org/10.1016/j.epsl.2015.08.024>  
 764 Campbell, B.A., Morgan, G.A., Whitten, J.L., Carter, L.M., Glaze, L.S., Campbell, D.B., 2017.  
 765 Pyroclastic flow deposits on Venus as indicators of renewed magmatic activity. J.  
 766 Geophys. Res. 122, 1580–1596. <https://doi.org/10.1002/2017JE005299>  
 767 Cassata, W.S., Renne, P.R., Shuster, D.L., 2011. Argon diffusion in pyroxenes: Implications  
 768 for thermochronometry and mantle degassing. Earth Planet. Sci. Lett. 304, 407–416.  
 769 <https://doi.org/10.1016/j.epsl.2011.02.019>  
 770 Coughlin, J.L., Mullally, F., Thompson, S.E., Rowe, J.F., Burke, C.J., Latham, D.W., Batalha,

N.M., Ofir, A., Quarles, B.L., Henze, C.E., Wolfgang, A., Caldwell, D.A., Bryson, S.T., Shporer, A., Catanzarite, J., Akeson, R., Barclay, T., Borucki, W.J., Boyajian, T.S., Campbell, J.R., Christiansen, J.L., Girouard, F.R., Haas, M.R., Howell, S.B., Huber, D., Jenkins, J.M., Li, J., Patil-Sabale, A., Quintana, E. V, Ramirez, S., Seader, S., Smith, J.C., Tenenbaum, P., Twicken, J.D., Zamudio, K.A., 2016. Planetary candidates observed by Kepler. vii. the first fully uniform catalog based on the entire 48-month data set (Q1-Q17 DR24). *Astrophys. J. Suppl. Ser.* 224. <https://doi.org/10.3847/0067-0049/224/1/12>

Davaille, A., Smrekar, S.E., Tomlinson, S., 2017. Experimental and observational evidence for plume-induced subduction on Venus. *Nat. Geosci.* 10, 349–. <https://doi.org/10.1038/ngeo2928>

Demouchy, S., 2010a. Diffusion of hydrogen in olivine grain boundaries and implications for the survival of water-rich zones in the Earth's mantle. *Earth Planet. Sci. Lett.* 295, 305–313. <https://doi.org/10.1016/j.epsl.2010.04.019>

Demouchy, S., 2010b. Hydrogen diffusion in spinel grain boundaries and consequences for chemical homogenization in hydrous peridotite. *Contrib. to Mineral. Petrol.* 160, 887–898. <https://doi.org/10.1007/s00410-010-0512-4>

Dittmann, J.A., Irwin, J.M., Charbonneau, D., Bonfils, X., Astudillo-Defru, N., Haywood, R.D., Berta-Thompson, Z.K., Newton, E.R., Rodriguez, J.E., Winters, J.G., Tan, T.-G., Almenara, J.-M., Bouchy, F., Delfosse, X., Forveille, T., Lovis, C., Murgas, F., Pepe, F., Santos, N.C., Udry, S., Wunsche, A., Esquerdo, G.A., Latham, D.W., Dressing, C.D., 2017. A temperate rocky super-Earth transiting a nearby cool star. *Nature* 544, 333–336. <https://doi.org/10.1038/nature22055>

Dorn, C., Noack, L., Rozel, A.B., 2018. Outgassing on stagnant-lid super-Earths. *Astron. Astrophys.* 614, A18. <https://doi.org/10.1051/0004-6361/201731513>

Dragomir, D., Teske, J., Gunther, M.N., Segransan, D., Burt, J.A., Huang, C.X., Vanderburg, A., Matthews, E., Dumusque, X., Stassun, K.G., Pepper, J., Ricker, E.R., Vanderspek,

798 R., Latham, D.W., Seager, S., Winn, J.N., Jenkins, J.M., Beatty, T., Bouchy, R., Brown,  
 799 T.M., Butler, R.P., Ciardi, A.R., Crane, J.D., Eastman, J.D., Fossati, L., Francis, J.,  
 800 Fulton, B.J., Gaudi, B.S., Goeke, R.F., James, D., Klaus, T.C., Kuhn, R.B., Lovis, C.,  
 801 Lund, M.B., McDermott, S., Paegert, M., Pepe, F., Rodriguez, J.E., Sha, L., Shectman,  
 802 S.A., Shporer, A., Siverd, R.J., Soto, A.G., Stevens, D.J., Twicken, J.D., Udry, S.,  
 803 Villanueva Jr., S., Wang, S.X., Wohler, B., Yao, X., Zhan, Z., 2019. TESS Delivers Its  
 804 First Earth-sized Planet and a Warm Sub-Neptune. *Astrophys. J. Lett.* 875. L7.  
 805 <https://doi.org/10.3847/2041-8213/ab12ed>  
 806 Elkins-Tanton, L.T., Smrekar, S.E., Hess, P.C., Parmentier, E.M., 2007. Volcanism and  
 807 volatile recycling on a one-plate planet: Applications to Venus. *J. Geophys. Res.* 112.  
 808 E04S06. <https://doi.org/10.1029/2006je002793>  
 809 Falloon, T.J., Green, D.H., 1989. The solidus of carbonated, fertile peridotite. *Earth Planet.*  
 810 *Sci. Lett.* 94, 364–370. [https://doi.org/10.1016/0012-821X\(89\)90153-2](https://doi.org/10.1016/0012-821X(89)90153-2)  
 811 Ferriss, E., Plank, T., Walker, D., 2016. Site-specific hydrogen diffusion rates during  
 812 clinopyroxene dehydration. *Contrib. to Mineral. Petrol.* 171.  
 813 <https://doi.org/10.1007/s00410-016-1262-8>  
 814 Filiberto, J., 2014. Magmatic diversity on Venus: Constraints from terrestrial analog  
 815 crystallization experiments. *Icarus* 231, 131–136.  
 816 <https://doi.org/10.1016/j.icarus.2013.12.003>  
 817 Foley, B.J., 2018. The dependence of planetary tectonics on mantle thermal state:  
 818 applications to early Earth evolution. *Philos. Trans. R. Soc. A-Mathematical Phys. Eng.*  
 819 *Sci.* 376. <https://doi.org/10.1098/rsta.2017.0409>  
 820 Foley, B.J., Driscoll, P.E., 2016. Whole planet coupling between climate, mantle, and core:  
 821 Implications for rocky planet evolution. *Geochemistry Geophys. Geosystems* 17, 1885–  
 822 1914. <https://doi.org/10.1002/2015GC006210>  
 823 Foley, B.J., Smye, A.J., 2018. Carbon Cycling and Habitability of Earth-Sized Stagnant Lid  
 824 Planets. *Astrobiology* 18, 873–896. <https://doi.org/10.1089/ast.2017.1695>



825 Frost, D.J., Liebske, C., Langenhorst, F., McCammon, C.A., Tronnes, R.G., Rubie, D.C.,  
826 2004. Experimental evidence for the existence of iron-rich metal in the Earth's lower  
827 mantle. *Nature* 428, 409–412.

828 Frost, D.J., McCammon, C.A., 2008. The redox state of Earth's mantle, in: *Annual Review of*  
829 *Earth and Planetary Sciences. Annual Reviews, Palo Alto*, pp. 389–420.  
830 <https://doi.org/10.1146/annurev.earth.36.031207.124322>

831 Ghail, R., 2015. Rheological and petrological implications for a stagnant lid regime on  
832 Venus. *Planet. Space Sci.* 113, 2–9. <https://doi.org/10.1016/j.pss.2015.02.005>

833 Gillon, M., Triaud, A.H.M.J., Fortney, J.J., Demory, B.-O., Jehin, E., Lendl, M., Magain, P.,  
834 Kabath, P., Queloz, D., Alonso, R., Anderson, D.R., Cameron, A.C., Fumel, A., Hebb,  
835 L., Hellier, C., Lanotte, A., Maxted, P.F.L., Mowlavi, N., Smalley, B., 2012. The Trappist  
836 survey of southern transiting planets I. Thirty eclipses of the ultra-short period planet  
837 WASP-43 b. *Astron. Astrophys.* 542. <https://doi.org/10.1051/0004-6361/201218817>

838 Greenwood, J.P., Karato, S., Vander Kaaden, K.E., Pahlevan, K., Usui, T., 2018. Water and  
839 Volatile Inventories of Mercury, Venus, the Moon, and Mars. *Space Sci. Rev.* 214.  
840 <https://doi.org/10.1007/s11214-018-0526-1>

841 Hayden, L.A., Watson, E.B., 2008. Grain boundary mobility of carbon in Earth's mantle: A  
842 possible carbon flux from the core. *Proc. Natl. Acad. Sci. U. S. A.* 105, 8537–8541.  
843 <https://doi.org/10.1073/pnas.0710806105>

844 Hirschmann, M.M., 2006. Water, melting, and the deep Earth H<sub>2</sub>O cycle. *Annu. Rev. Earth*  
845 *Planet. Sci.* 34, 629–653.

846 Hiscock, M., 2013. The importance of grain boundary diffusion: An experimental study. PhD  
847 thesis, University of Edinburgh. 312 pages.  
848 <https://pdfs.semanticscholar.org/8a86/afa07ed8428d86735af7118ad15d293ba9a0.pdf>

849 Ingrin, J., Skogby, H., 2000. Hydrogen in nominally anhydrous upper-mantle minerals:  
850 concentration levels and implications. *Eur. J. Mineral.* 12, 543–570.

851 Ivanov, M.A., 2015. Volcanic complexes on Venus: Distribution, age, mechanisms of origin,

and evolution. *Petrology* 23, 127–149. <https://doi.org/10.1134/S0869591115020046>

Ivanov, M.A., Head, J.W., 2015. The history of tectonism on Venus: A stratigraphic analysis. *Planet. Space Sci.* 113, 10–32. <https://doi.org/10.1016/j.pss.2015.03.016>

Johnson, C.L., Hauck II, S.A., 2016. A whole new Mercury: Messenger reveals a dynamic planet at the last frontier of the inner solar system. *J. Geophys. Res.* 121, 2349–2362. <https://doi.org/10.1002/2016JE005150>

Johnson, E.A., Rossman, G.R., 2013. The diffusion behavior of hydrogen in plagioclase feldspar at 800–1000°C: Implications for re-equilibration of hydroxyl in volcanic phenocrysts. *Am. Mineral.* 98, 1779–1787. <https://doi.org/10.2138/am.2013.4521>

Kane, S.R., Ceja, A.Y., Way, M.J., Quintana, E. V, 2018. Climate Modeling of a Potential ExoVenus. *Astrophys. J.* 869. <https://doi.org/10.3847/1538-4357/aaec68>

Kaula, W.M., 1999. Constraints on Venus evolution from radiogenic argon. *Icarus* 139, 32–39. <https://doi.org/10.1006/icar.1999.6082>

Lecuyer, C., Simon, L., Guyot, F., 2000. Comparison of carbon, nitrogen and water budgets on Venus and the Earth. *Earth Planet. Sci. Lett.* 181, 33–40. [https://doi.org/10.1016/S0012-821X\(00\)00195-3](https://doi.org/10.1016/S0012-821X(00)00195-3)

Maaloe, S., 2004. The solidus of harzburgite to 3 GPa pressure: the compositions of primary abyssal tholeiite. *Mineral. Petrol.* 81, 1–17. <https://doi.org/10.1007/s00710-004-0028-6>

Mackwell, S.J., Kohlstedt, D.L., 1990. Diffusion of hydrogen in olivine: Implications for water in the mantle. *J. Geophys. Res.* 95, 5079–5088.

Marty, B., Altwegg, K., Balsiger, H., Bar-Nun, A., Bekaert, D. V, Berthelier, J.-J., Bieler, A., Briois, C., Calmonte, U., Combi, M., De Keyser, J., Fiethe, B., Fuselier, S.A., Gasc, S., Gombosi, T.I., Hansen, K.C., Haessig, M., Jaeckel, A., Kopp, E., Korth, A., Le Roy, L., Mall, U., Mousis, O., Owen, T., Reme, H., Rubin, M., Semon, T., Tzou, C.-Y., Waite, J.H., Wurz, P., 2017. Xenon isotopes in 67P/Churyumov-Gerasimenko show that comets contributed to Earth's atmosphere. *Science*. 356, 1069–1072. <https://doi.org/10.1126/science.aal3496>

879 Mikhail, S., Heap, M.J., 2017. Hot climate inhibits volcanism on Venus: Constraints from rock  
880 deformation experiments and argon isotope geochemistry. *Phys. Earth Planet. Inter.*  
881 268, 18–34. <https://doi.org/10.1016/j.pepi.2017.05.007>

882 Nimmo, F., McKenzie, D., 1998. Volcanism and tectonics on Venus. *Annu. Rev. Earth*  
883 *Planet. Sci.* 26, 23–51. <https://doi.org/10.1146/annurev.earth.26.1.23>

884 Noack, L., Rivoldini, A., Van Hoolst, T., 2017. Volcanism and outgassing of stagnant-lid  
885 planets: Implications for the habitable zone. *Phys. EARTH Planet. Inter.* 269, 40–57.  
886 <https://doi.org/10.1016/j.pepi.2017.05.010>

887 O'Rourke, J.G., Korenaga, J., 2015. Thermal evolution of Venus with argon degassing.  
888 *Icarus* 260, 128–140. <https://doi.org/10.1016/j.icarus.2015.07.009>

889 O'Rourke, J.G., Korenaga, J., 2012. Terrestrial planet evolution in the stagnant-lid regime:  
890 Size effects and the formation of self-destabilizing crust. *Icarus* 221, 1043–1060.  
891 <https://doi.org/10.1016/j.icarus.2012.10.015>

892 Padron-Navarta, J.A., Hermann, J., O'Neill, H.S.C., 2014. Site-specific hydrogen diffusion  
893 rates in forsterite. *Earth Planet. Sci. Lett.* 392, 100–112.  
894 <https://doi.org/10.1016/j.epsl.2014.01.055>

895 Peslier, A.H., 2010. A review of water contents of nominally anhydrous natural minerals in  
896 the mantles of Earth, Mars and the Moon. *J. Volcanol. Geotherm. Res.* 197, 239–258.  
897 <https://doi.org/10.1016/j.jvolgeores.2009.10.006>

898 Plesa, A.-C., Padovan, S., Tosi, N., Breuer, D., Grott, M., Wieczorek, M.A., Spohn, T.,  
899 Smrekar, S.E., Banerdt, W.B., 2018. The Thermal State and Interior Structure of Mars.  
900 *Geophys. Res. Lett.* 45, 12198–12209. <https://doi.org/10.1029/2018GL080728>

901 Rauch, M., Keppler, H., 2002. Water solubility in orthopyroxene. *Contrib. to Mineral. Petrol.*  
902 143, 525–536.

903 Rohrbach, A., Ballhaus, C., Golla-Schindler, U., Ulmer, P., Kamenetsky, V.S., Kuzmin, D. V.,  
904 2007. Metal saturation in the upper mantle. *Nature* 449, 456–458.  
905 <https://doi.org/10.1038/nature06183>

906 Rolf, T., Steinberger, B., Sruthi, U., Werner, S.C., 2018. Inferences on the mantle viscosity  
 907 structure and the post-overtun evolutionary state of Venus. *Icarus* 313, 107–123.  
 908 <https://doi.org/10.1016/j.icarus.2018.05.014>  
 909 Rushby, A.J., Johnson, M., Mills, B.J.W., Watson, A.J., Claire, M.W., 2018. Long-Term  
 910 Planetary Habitability and the Carbonate-Silicate Cycle. *Astrobiology* 18, 469–480.  
 911 <https://doi.org/10.1089/ast.2017.1693>  
 912 Saal, A., Hauri, E., Lo Cascio, M., Van Orman, J.A., Rutherford, M.C., Cooper, A.R., 2008.  
 913 Volatile content of lunar volcanic glasses and the presence of water in the Moon's  
 914 interior. *Nature* 454, 192-195.  
 915 Saal, A.E., Hauri, E.H., Van Orman, J.A., Rutherford, M.J., 2013. Hydrogen Isotopes in  
 916 Lunar Volcanic Glasses and Melt Inclusions Reveal a Carbonaceous Chondrite  
 917 Heritage. *Science*. 340, 1317–1320. <https://doi.org/10.1126/science.1235142>  
 918 Schubert, G., Sandwell, D.T., 1995. A global survey of possible subduction sites on venus.  
 919 *Icarus* 117, 173–196. <https://doi.org/10.1006/icar.1995.1150>  
 920 Shahr, A., Driscoll, P., Weinberger, A., Cody, G., 2019. Planetary science: What makes a  
 921 planet habitable? *Science*. 364, 434–435. <https://doi.org/10.1126/science.aaw4326>  
 922 Smrekar, S.E., Davaille, A., Sotin, C., 2018. Venus Interior Structure and Dynamics. *Space*  
 923 *Sci. Rev.* 214. <https://doi.org/10.1007/s11214-018-0518-1>  
 924 Smrekar, S.E., Sotin, C., 2012. Constraints on mantle plumes on Venus: Implications for  
 925 volatile history. *Icarus* 217, 510–523. <https://doi.org/10.1016/j.icarus.2011.09.011>  
 926 Smyth, J.R., Frost, D.J., Nestola, F., Holl, C.M., Bromiley, G.D., 2006. Olivine hydration in  
 927 the deep upper mantle: Effects of temperature and silica activity. *Geophys. Res. Lett.*  
 928 33, L15301.  
 929 Solomatov, V.S., Moresi, L.N., 1996. Stagnant lid convection on Venus. *J. Geophys. Res.*  
 930 101, 4737–4753. <https://doi.org/10.1029/95JE03361>  
 931 Stalder, R., Behrens, H., 2006. D/H exchange in pure and Cr-doped enstatite: implications  
 932 for hydrogen diffusivity. *Phys. Chem. Miner.* 33, 601–611.

933 Stalder, R., Purwin, H., Skogby, H., 2007. Influence of Fe on hydrogen diffusivity in  
 934 orthopyroxene. *Eur. J. Mineral.* 19, 899–903. [https://doi.org/10.1127/0935-](https://doi.org/10.1127/0935-1221/2007/0019-1780)  
 935 1221/2007/0019-1780  
 936 Stalder, R., Skogby, H., 2003. Hydrogen diffusion in natural and synthetic orthopyroxene.  
 937 *Phys. Chem. Miner.* 30, 12–19.  
 938 Sundvall, R., Skogby, H., Stalder, R., 2009. Dehydration-hydration mechanisms in synthetic  
 939 Fe-poor diopside. *Eur. J. Mineral.* 21, 17–26. [https://doi.org/10.1127/0935-](https://doi.org/10.1127/0935-1221/2009/0021-1880)  
 940 1221/2009/0021-1880  
 941 Thomas, J.B., Cherniak, D.J., Watson, E.B., 2008. Lattice diffusion and solubility of argon in  
 942 forsterite, enstatite, quartz and corundum. *Chem. Geol.* 253, 1–22.  
 943 <https://doi.org/10.1016/j.chemgeo.2008.03.007>  
 944 Tolstikhin, I., Kamensky, I., Tarakanov, S., Kramers, J., Pekala, M., Skiba, V., Gannibal, M.,  
 945 Novikov, D., 2010. Noble gas isotope sites and mobility in mafic rocks and olivine.  
 946 *Geochim. Cosmochim. Acta* 74, 1436–1447. <https://doi.org/10.1016/j.gca.2009.11.001>  
 947 Tosi, N., Godolt, M., Stracke, B., Ruedas, T., Grenfell, J.L., Hoening, D., Nikolaou, A., Plesa,  
 948 A.-C., Breuer, D., Spohn, T., 2017. The habitability of a stagnant-lid Earth. *Astron.*  
 949 *Astrophys.* 605. <https://doi.org/10.1051/0004-6361/201730728>  
 950 Trull, T. W., 1981. Diffusion of helium isotopes in silicate glasses and minerals: implications  
 951 for petrogenesis and geochronology. PhD Thesis, 1918-04, Massachusetts Institute of  
 952 Technology. DOI:10.1575/1912/5399, <https://hdl.handle.net/1912/5399>  
 953 van Summeren, J., Conrad, C.P., Gaidos, E., 2011. Mantle convection, plate tectonics, and  
 954 volcanism on hot exo-earths. *Astrophys. J. Lett.* 736. [https://doi.org/10.1088/2041-](https://doi.org/10.1088/2041-8205/736/1/L15)  
 955 8205/736/1/L15  
 956 Veeder, G.J., Davies, A.G., Matson, D.L., Johnson, T. V, 2009. Io: Heat flow from dark  
 957 volcanic fields. *Icarus* 204, 239–253. <https://doi.org/10.1016/j.icarus.2009.06.027>  
 958 Wetherill GW, 1986. Accumulation of the terrestrial planets and implications concerning  
 959 lunar origin, in: *Origin of the Moon*. Lunar and Planetary Institute, pp. 519–550.

960 Wieczorek, M.A., Jolliff, B.L., Khan, A., Pritchard, M.E., Weiss, B.P., Williams, J.G., Hood,  
961 L.L., Richter, K., Neal, C.R., Shearer, C.K., McCallum, I.S., Tompkins, S., Hawke, B.R.,  
962 Peterson, C., Gillis, J.J., Bussey, B., 2006. The constitution and structure of the lunar  
963 interior, in: Jolliff, BL and Wieczorek, MA (Ed.), New views of the moon, Reviews in  
964 Mineralogy & Geochemistry. Mineralogical Soc Amer & Geochemical Soc, 3635  
965 Concorde Pkwy STE 500, Chantilly, VA 20151-1125 USA, p. 221+.  
966 <https://doi.org/10.2138/rmg.2006.60.3>  
967 Wordsworth, R.D., 2016. Atmospheric nitrogen evolution on Earth and Venus. Earth Planet.  
968 Sci. Lett. 447, 103–111. <https://doi.org/10.1016/j.epsl.2016.04.002>  
969

**Figure 1. Simplified stagnant-lid regime model used in this study. Text denotes composition of each part of the stagnant lid. Convecting mantle is assumed to be an infinite reservoir for each volatile species (direction of flux shown by arrow).**

**Figure 2. Top: 4 model Venusian temperature profiles used to constrain variations in temperature with depth across the model stagnant lid. See text for detailed descriptions of each. Dashed grey lines are 5, 6 and 7 K/km geothermal gradients based on a Venusian surface temperature of 735 K. Bottom: calculated effective diffusivity for H for each modelled temperature profile, assuming fast lattice diffusion in an oxidised stagnant lid.**

**Figure 3. Graphical representation of box modelling procedure used. A) depth (D), temperature (T) and concentration of species (X) data used as the input to the first time step in the model. B) shows a representative concentration (i.e. diffusion) profile after time  $t$ . This concentration profile is then used as the input into the second time step C), over which concentration changes in two shells are then modelled. D) The output from the second time step is then used as the input into the next time step E). This procedure is repeated upwards through the model.**

**Figure 4. H concentration profiles through the model stagnant lid after  $t=100, 250, 500, 1000$  and  $2000$  Myr (from right to left) based on the Nimmo and McKenzie (1998) temperature profile for Venus (black line). For comparison, the light grey line shows a concentration profile based on an ‘infinite source’ solution to Fick’s second law after 2 Gyr (see text for details). Grey solid line marks the  $H_2O$  storage capacity of the lid, based on solubility of  $H_2O$  in orthopyroxene and olivine (Bolfan-Casanova, 2005). At water contents exceeding this value a free fluid phase or hydrous melt will be present. Thin black line marks the hazburgite solidus (Maaloe, 2004), and dashed black lines**

denote the dry mantle (peridotite) solidus, and calculated effect of H<sub>2</sub>O on depression of the mantle solidus from Hirschmann (2006).

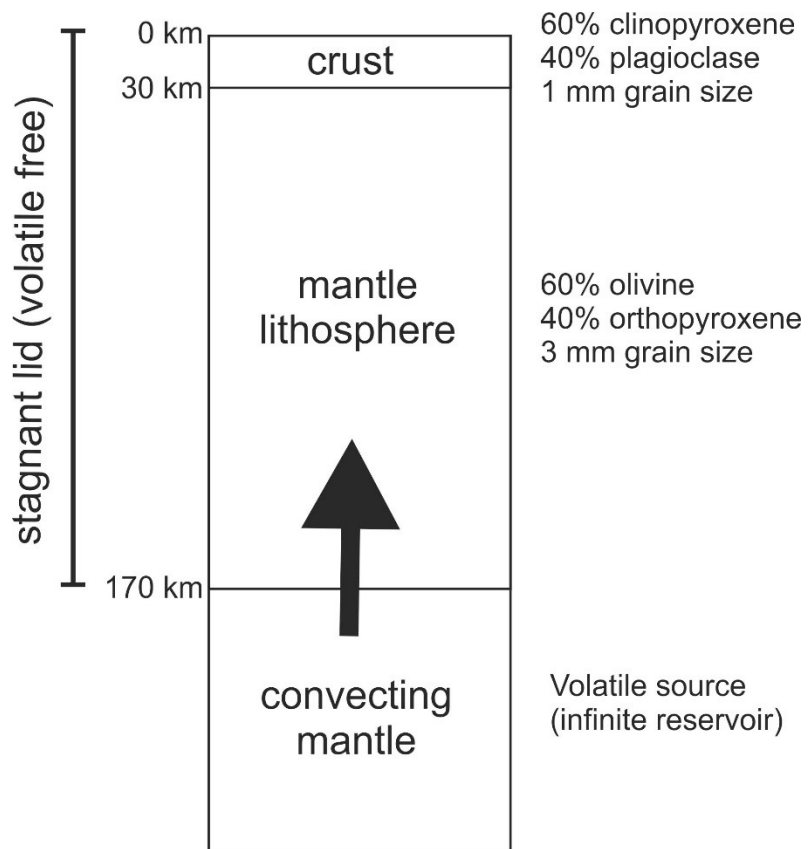
**Figure 5. Comparison of concentration profiles for H<sub>2</sub>O (both fast and slow H diffusion), C diffusion (by grain boundary diffusion only), He diffusion and Ar diffusion after 2 Gyr calculated based on a Nimmo and McKenzie (1998) Venusian temperature profile.**

**Figure 6. Fast H concentration profiles through the model stagnant lid based on Venusian geotherms from Ghail et al. (2015). A. Black lines are model geotherms (Ghail, 2015) for an ambient stagnant lid (12 mWm<sup>-2</sup>) and a lid heated by thermal plumes (36 mWm<sup>-2</sup> for the centre of plume head; 18 mWm<sup>-2</sup> for a region adjacent to a mature plume). H concentration profiles for same time steps as Fig. 4 are based on a 18 mWm<sup>-2</sup> geotherm. Grey lines and shaded fields mark melt relations in carbonated peridotite from Ghail (2015). B. H concentration profiles for a 12 mWm<sup>-2</sup> geotherm. C. H concentration profiles for a Ghail (2015) 18 mWm<sup>-2</sup> geotherm for initial stagnant lid water contents of 200 ppm.**

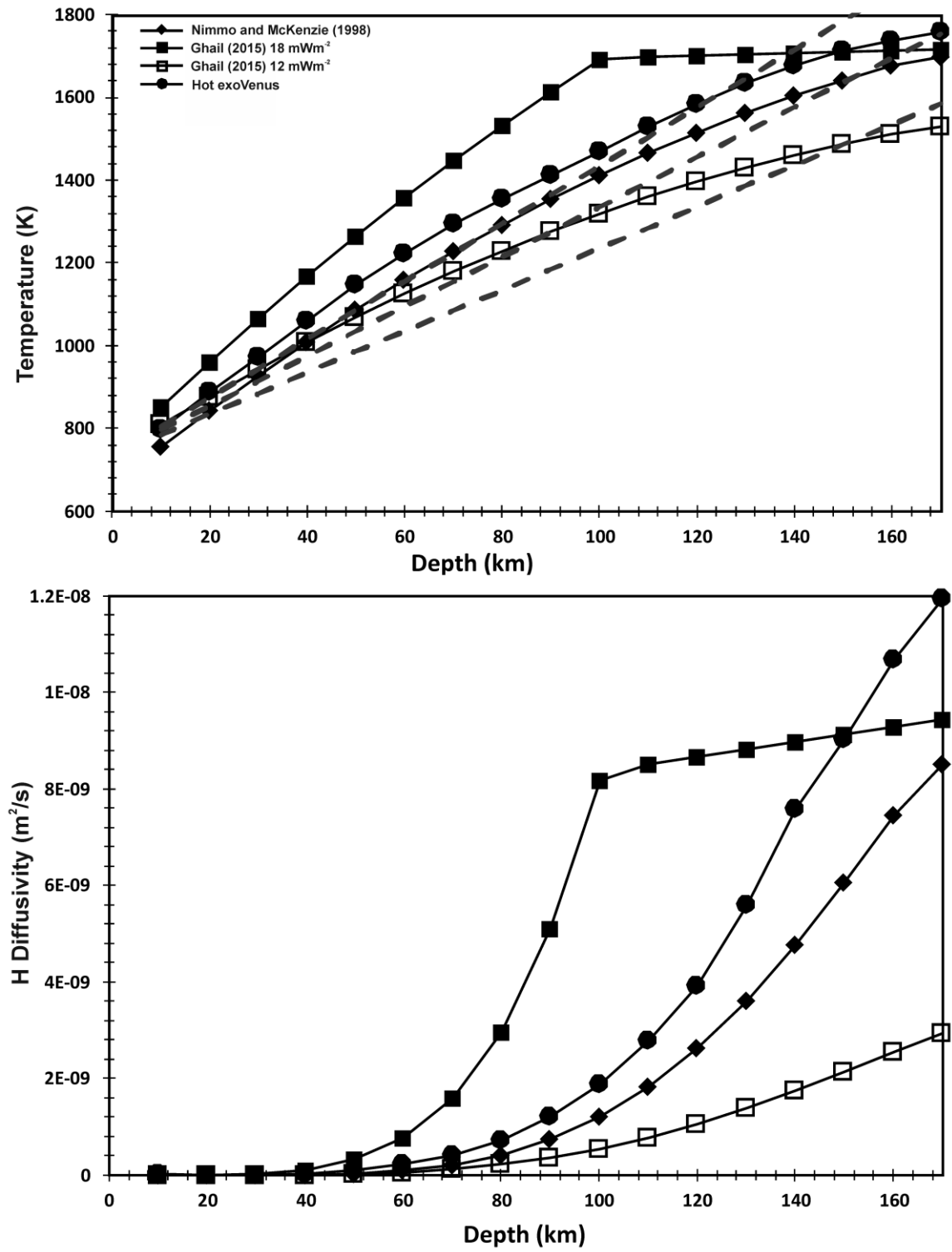
**Figure 7. H<sub>2</sub>O concentration profiles based on a hypothetical ‘hot Venusian’ geotherm, or hot stagnant lid. Key same as figure 4.**



**Figure 1**

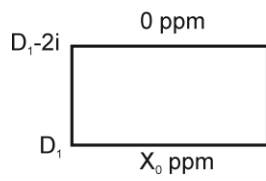


1035 **Figure 2**  
1036

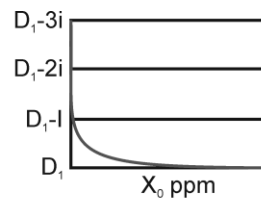


1037  
1038

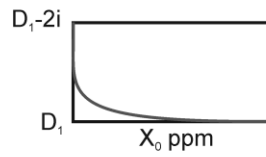
**Figure 3**



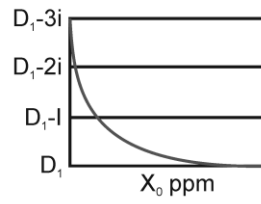
**A) Initial Model Input**



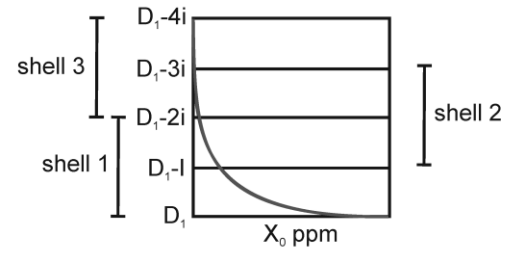
**C) Input to time-step 2**



**B) Output after time-step 1**

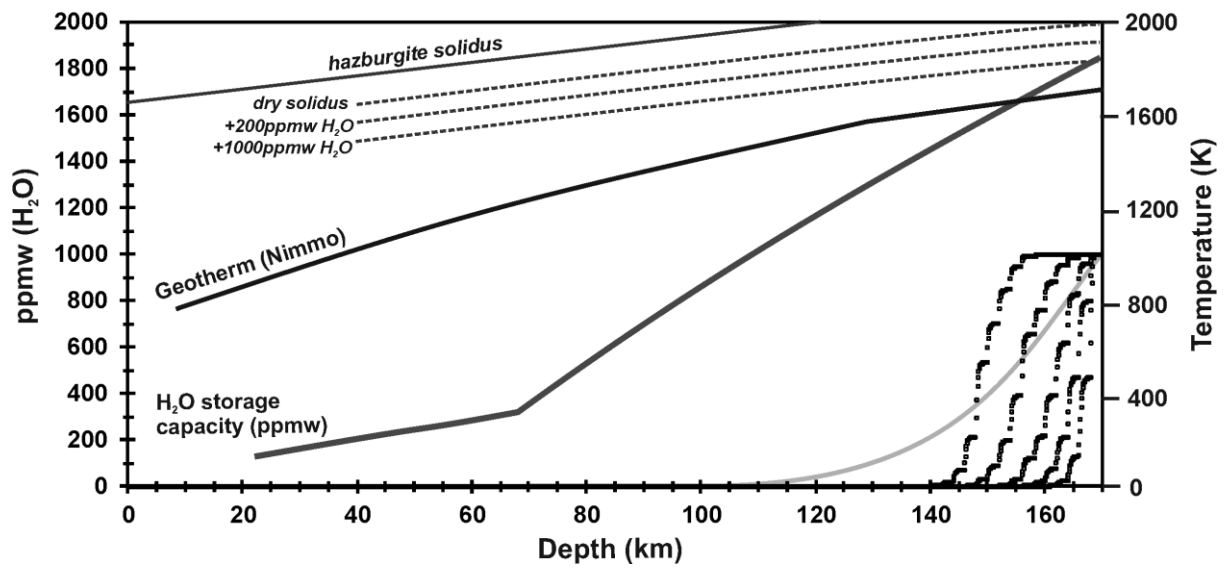


**D) Output after time-step 2**

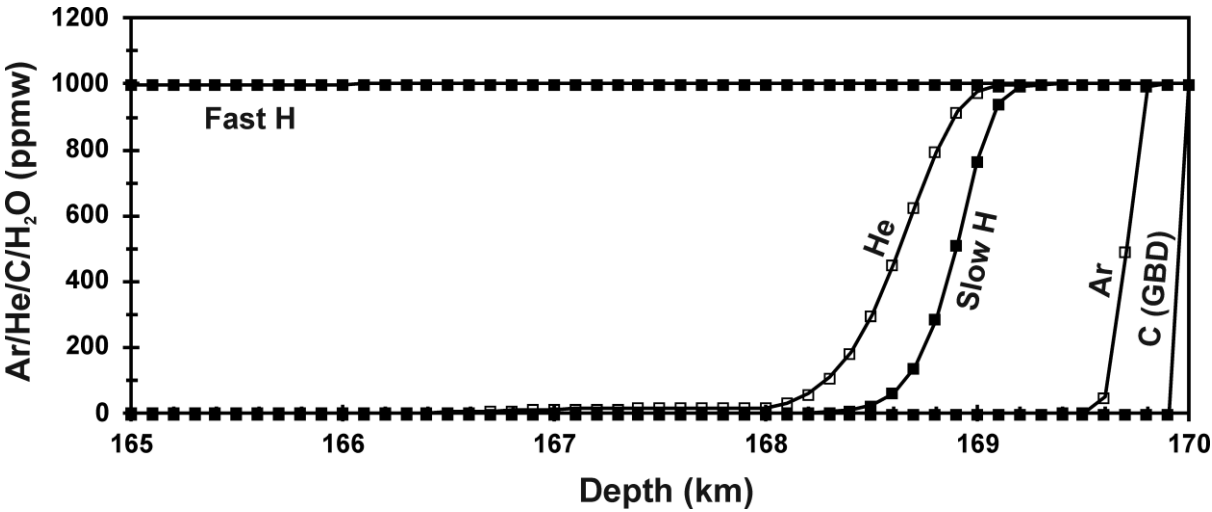


**E) Input to time-step 3**

**Figure 4**

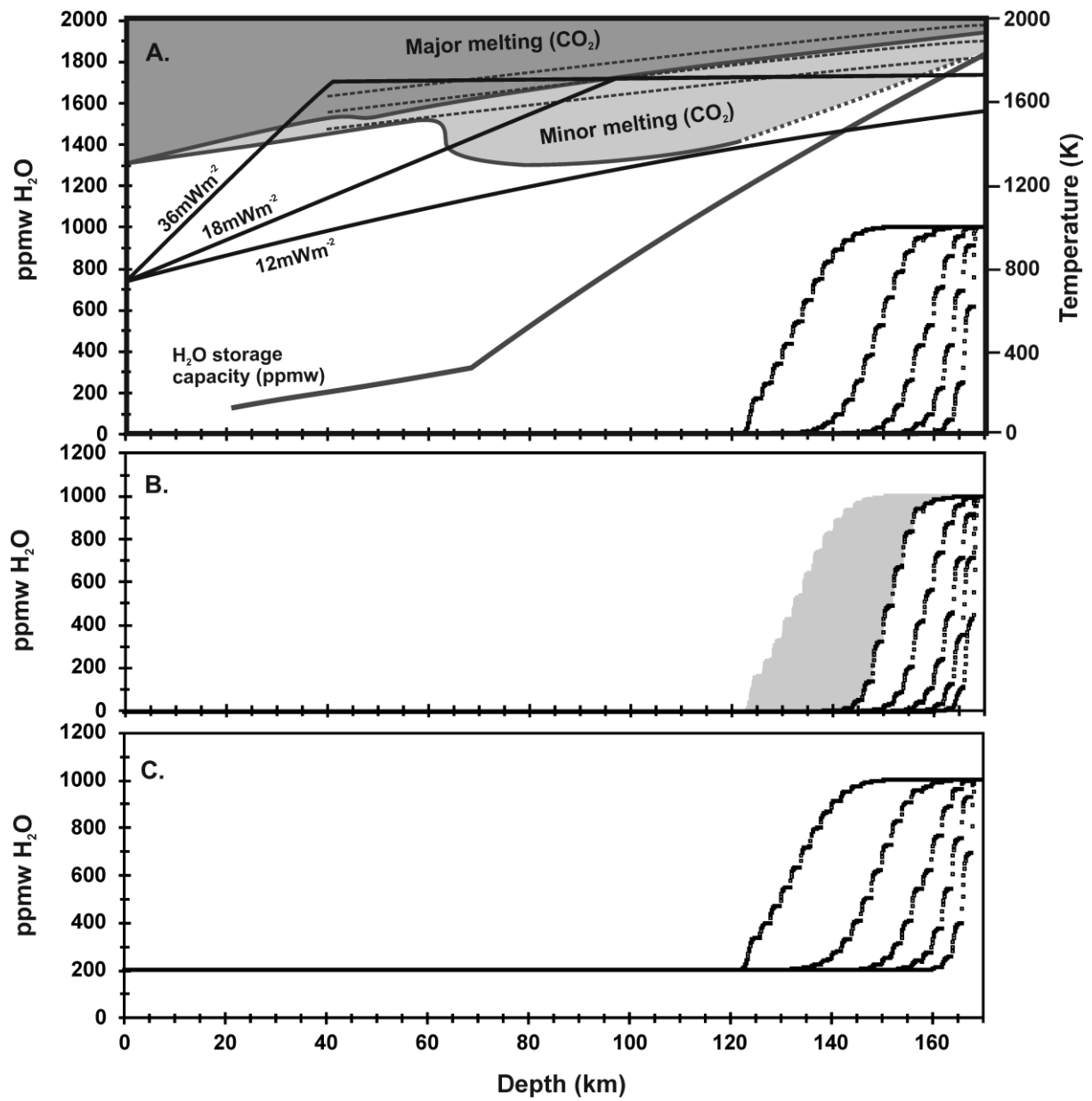


1051 **Figure 5**  
1052

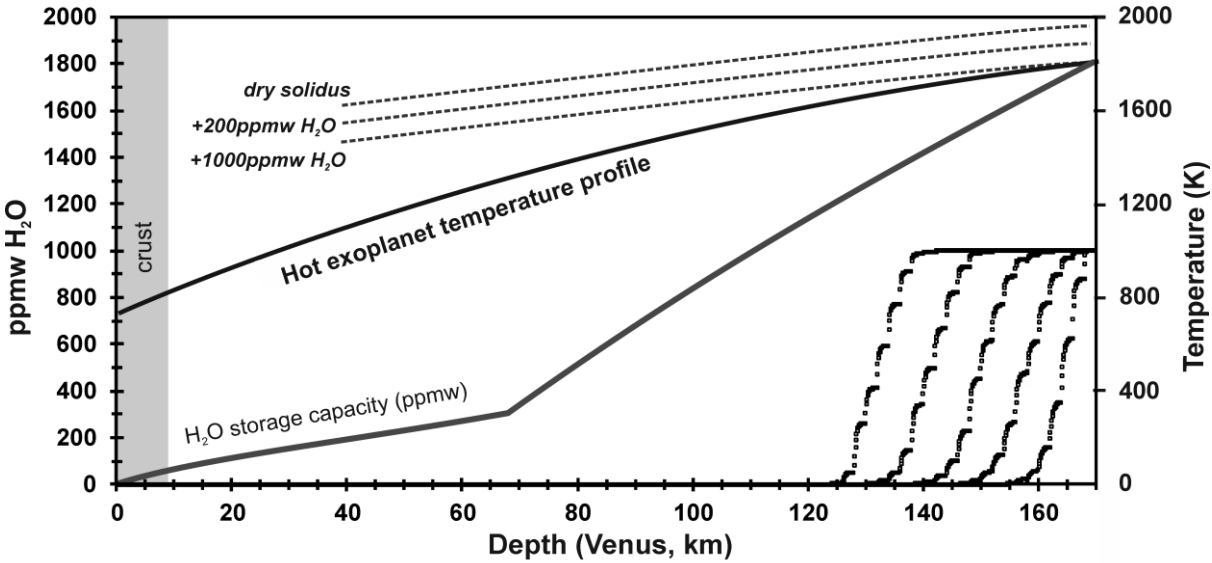


1053  
1054  
1055

**Figure 6**



1063 **Figure 7**  
1064



1065